Open- and Closed-Loop Dynamics of the High-Efficiency Antenna Subreflector

M. B. Kuczenski[1] and W. Gawronski[2]

The subreflector of the high-efficiency (HEF) antenna moves in three axes, while the subreflector controller supervises these movements. The precision of subreflector response to the controller commands is essential to maintaining the antenna-pointing precision. This article presents the development of the control system model of the HEF antenna subreflector. It includes the dynamics of the open-loop (or rate-loop) system, the development of the controller, and the simulations of the closed-loop performance. The analysis shows that the closed-loop dynamics, such as settling time, overshoot, and bandwidth, are comparable to the antenna closed-loop dynamics; thus, they are able to meet the pointing requirements.

I. Introduction

Due to gravity loading of the antenna structure, the subreflector movement in three axes is tied to the antenna elevation movement to maintain the correct focal point. The movement is supervised by the subreflector controller. Its precision and dynamics are essential to maintaining the antenna-pointing precision. This article discusses the development of the Simulink model for the DSS-15 subreflector controller, presents the performance of the open-loop (or rate-loop) system, describes the controller, and presents the closed-loop performance.

II. Description of the Subreflector Assembly

The following description is based on JPL drawings[3] and the authors' on-site inspections. The subreflector moves in three axes, called the x-, y-, and z-axes. Their orientation is shown in Fig. 1. Each axis has a total travel of 152 mm (6.0 in.). The x-axis corresponds to left–right motion of the subreflector (motion parallel to the elevation axis of rotation). The z-axis moves the subreflector along the axis directed from the subreflector vertex to the focal point of the main dish. The y-axis corresponds to movement of the subreflector along the axis orthogonal to the x- and z-axes. In other words, when lying face-up on the

[1] Cooperative Education Program student, University of California, Berkeley.

[2] Communications Ground Systems Section.

[3] "Subreflector Positioner Assy, 34m Antenna," rev. B, JPL Mechanical Drawing 9479988 (internal document), Jet Propulsion Laboratory, Pasadena, California, 1983, and rev. C, engineering pre-release, p. 1.

The research described in this publication was carried out by the Jet Propulsion Laboratory, California Institute of Technology, under a contract with the National Aeronautics and Space Administration.

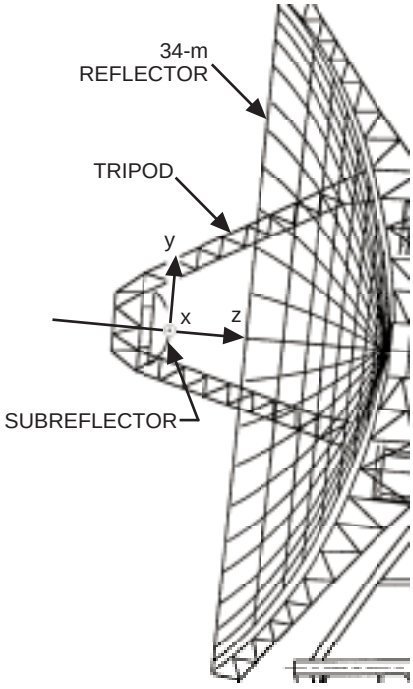

Fig. 1. Description of the axes for subreflector motion.

surface of the dish with feet pointed downward with the dish tipped, the x-axis direction would be left to right, the y-axis direction would be head to toe, and the z-axis direction would move the subreflector vertically, closer to or farther from your face. See Fig. 1 for a clarification of this hardware arrangement.

There is a total of five motors in the subreflector positioner assembly: one each for the x- and y-axes and three independently controlled motors for the z-axis, located in a circular pattern, 120 deg apart from one another. All five motors are Baldor model 3320 1/3 hp (185 W) DC motors.

Subreflector positioning is implemented using three parallel plates, referred to as "top," "center," and "bottom" by means of their relative orientation when the antenna is pointed straight up (an elevation angle of 90 deg). The subreflector motors are arranged as follows:

(1) The three z-axis motors are mounted on the bottom plate. The subreflector itself is attached to the inboard side of the bottom plate and moves in the z-axis relative to the bottom plate.

(2) The x-axis motor is mounted on the center plate; the subreflector and bottom plate move together in the x-axis, relative to the center plate.

(2) The y-axis motor is mounted on the top plate, which is rigidly fixed to the antenna quadripod assembly. The subreflector and the center and bottom plates move together in the y-axis relative to the top plate.

The y-axis motor and drive components are mounted to the top plate; the x-axis motor and components are affixed to the center plate; and the z-axis motor and components are attached to the bottom plate. The three plates are attached together with linear bearings.

The outputs of the motors are each attached to gear reducers in the ratio of 6.3 to 1, which are in turn connected to ball screw actuators to further gear down the motor motions. The ball screws for the z- and

x-axes have ratios of 37.8 revolutions per centimeter, while the ball screw for the y-axis has a ratio of 22.9 revolutions per centimeter. A lower-ratio ball screw on the y-axis allows for faster movement of the subreflector to compensate more quickly for gravity loading effects, which would naturally be manifest in the vertical (y-axis) direction.

Position feedback is obtained from five independent hermetically sealed linear velocity differential transducers (LVDTs) mounted adjacent to the ball screw actuators. The transducers measure the relative motions between the plates, as described previously. Rate-loop feedback is obtained from tachometers that are integral parts of the drive motors.

The amplifiers control the motor movements. They are manufactured by EG&G Torque Systems.[4] Each amplifier consists of a linear operational amplifier circuit that is represented in the model as a second-order discrete transfer function.[5] It contains an internally closed current loop that is equivalent to a closed torque loop for the purposes of simulation and control.

III. Modeling of the Subreflector Rate Loop

It was considered desirable to create a simulation model of the subreflector open-loop (or rate-loop) system that accurately represented the motion of the real subreflector prior to designing a controller. The model was based on the mechanical layout described above and was implemented in Simulink. Figure 2 shows the Simulink representation of the closed-loop control system and the location of the rate loop within that system.

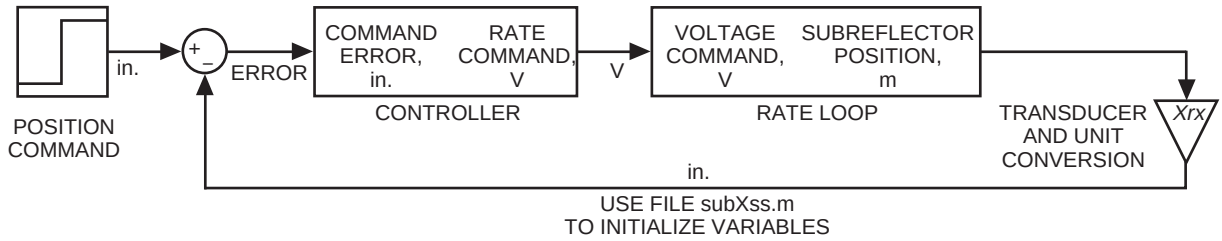

Fig. 2. Simulink model of the closed-loop system.

Shown in Fig. 3 is the Simulink model created for the subreflector rate loop. It consists of the amplifier, motor, and mechanical subsystem and contains the torque feedback loop within it. The model is entirely parameter-based, with no numerical values built-in, except for the unit conversion factors. This architecture allows the user to define different parameters for the model in an outside file and to load and modify these values without altering the Simulink model at all.

A. Amplifier

The amplifier model is shown in Fig. 4. The transfer function of its first component is generated from electrical circuit parameters. Given the existing parameters and presently installed components, the amplifier continuous time transfer function is as follows:

$$G_{\text{amp}} = \frac{0.000491s + 4.91}{8.946 \times 10^{-6}s^2 + 0.08956s + 1} \tag{1}$$

[4] The amplifiers are described in detail in *Antenna and Subreflector Servo Assemblies, 34m Az-El Antenna*, TMOD Document TM 08601 (internal document), Appendix B, Jet Propulsion Laboratory, Pasadena, California, 1987.

[5] Ibid. Based on the description in Appendix B, pp. 7–9.

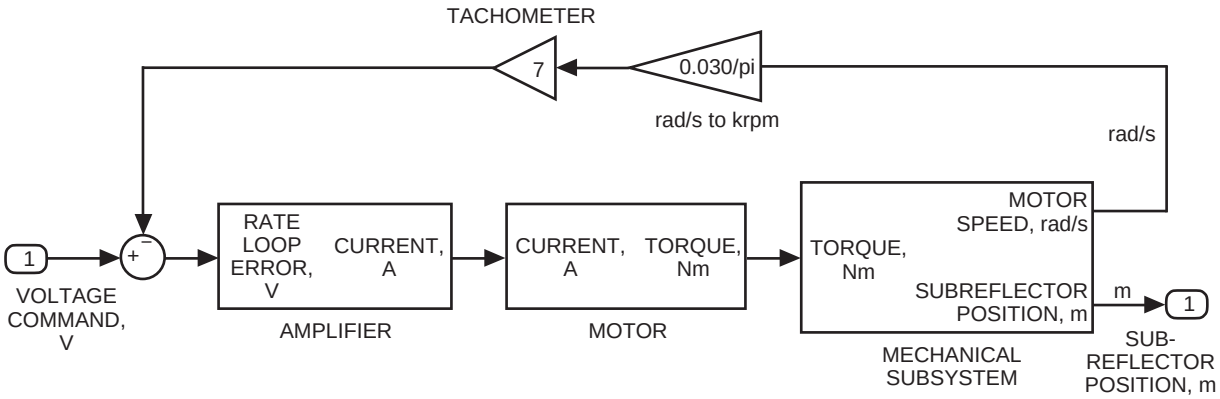

Fig. 3. Simulink model of the rate-loop system.

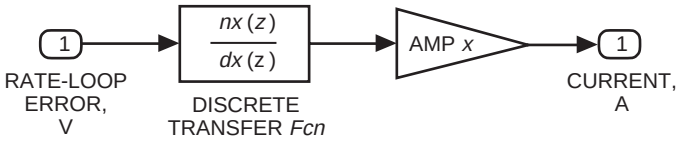

Fig. 4. Simulink model of the amplifier circuit.

The Bode plot for the transfer function is shown in Fig. 5. The second component is a voltage-to-current amplification stage with a gain of 2.4 A/V.[6] The amplifier is linear up to 50 V of output voltage or 20 peak A of output current.

B. Motor

The subreflector motors, Baldor model 3320, are rated for 185 W output at 90 V and 1750 rpm. The motors were modeled as linear converters of input current into output torque, with gain K_t. The torque constant, K_t; speed constant; armature resistance; and shaft damping were calculated from experimental data acquired from the manufacturer. The test data, given in Table 1, included the device's speed, voltage, and current draw at no-load and full-load (1.356 Nm or 1 lb-ft) conditions.

In the following standard relationships,

$$V_{\text{arm}} = I_{\text{arm}} R + K_b \omega \tag{2a}$$

$$I_{\text{arm}} K_t = T + B\omega \tag{2b}$$

The V_{arm} and I_{arm} are the voltage and current, respectively, across the motor's armature; T is the load; and ω is the shaft speed. There are four unknown parameters: K_b and K_t, the motor speed and torque constants, respectively; B, the motor's shaft damping coefficient; and R, the armature resistance. With two tests and two equations for each test, the four unknown quantities are determined. Using the lowest speed in the stated range gave the most conservative results, which are given in Table 2. As a result, the sought-after torque constant, K_t, was calculated to be 0.422 Nm/A.

C. Mechanical Subsystem

The model of the mechanical subsystem, represented in Simulink as a six-dimensional linear state–space model, is shown in Fig. 6. The subsystem consists of the gearbox, ball screw, and the subreflector.

[6] Ibid. See Appendix B, p. 7.

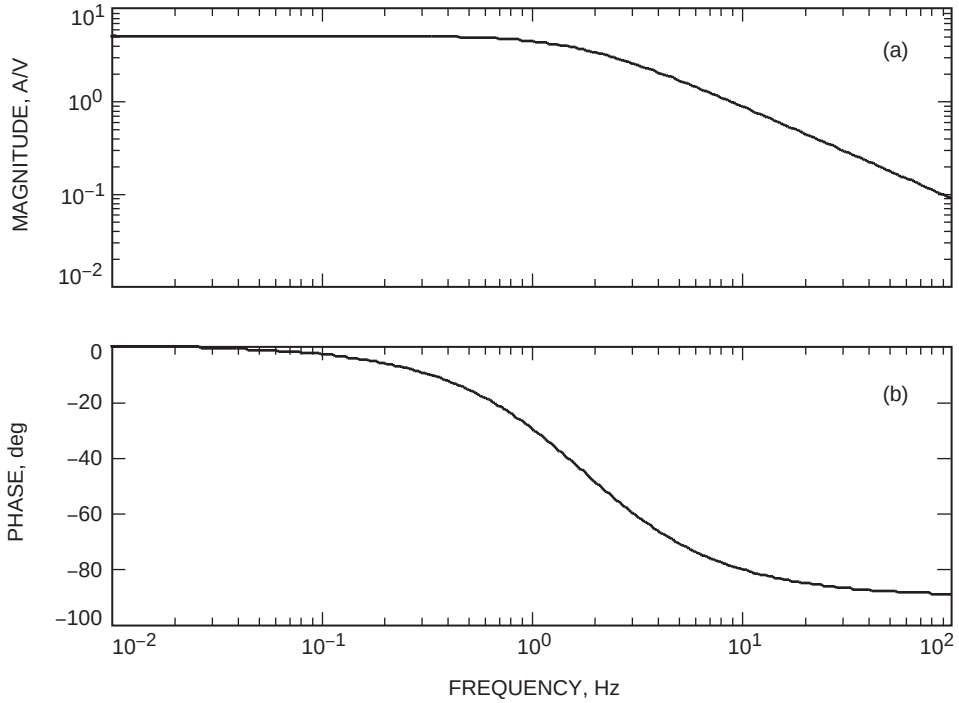

Fig. 5. Transfer function of the amplifier circuit: (a) magnitude and (b) phase.

Table 1. Motor test data.

Test case	Armature voltage, V_{arm}, V	Armature current, I_{arm}, A	Motor torque, T, Nm	Motor speed, ω, rad/s
No load	90.0	0.40	0	182–202
Full load	90.0	3.55	1.356	159–186

Table 2. Motor parameters.[a]

Parameter	Value
Speed constant, K_b	0.486 V/rad
Torque constant, K_t	0.422 Nm/A
Resistance, R	3.5 Ω
Inductance,[b] L	0.0162 H
Damping, B_m	0.00092 Nms/rad
Shaft inertia,[b] J_s	0.003 kgm^2
Tachometer constant	7.0 V per 1000 rpm

[a] Motor rating: 249 W (or 1/3 hp) at 90 V and 183 rad/s (or 1750 rpm).

[b] From the Baldor catalog.

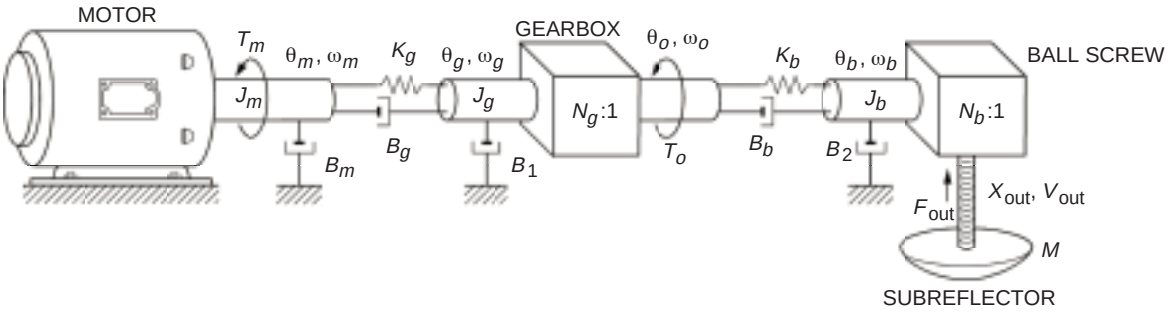

Fig. 6. Schematic of the subreflector drive model.

The input stiffness gearbox model (Fig. 7) was used in this simulation, not the output stiffness model in Fig. 8. It accounts for flexibility in the gearboxes and actuators. In this model, the gearbox is represented as a spring-mass-damper system attached to a rigid gear reducer.

The state equations for the gear reducer variables are derived from balance-of-torque equations:

$$T_m = J_m\dot{\omega}_m + B_m\omega_m + k_g(\theta_m - \theta_g) + B_g(\omega_m - \omega_g) \tag{3a}$$

$$J_g\dot{\omega}_g + B_1\omega_g = k_g(\theta_m - \theta_g) + B_g(\omega_m - \omega_g) + \frac{T_o}{N_g} \tag{3b}$$

where θ_m and ω_m are motor angle and rate, respectively; θ_g and ω_g are gearbox input angle and rate, respectively; θ_o and ω_o are gearbox output angle and rate, respectively; $\theta_g = N_g\theta_o$; and $\omega_g = N_g\omega_o$. The variable T_o represents feedback of the torque required downstream from the gearbox:

$$T_o = k_b(\theta_b - \theta_o) + B_b(\omega_b - \omega_o) \tag{3c}$$

where θ_b and ω_b are the ball screw input angle and rate, respectively.

There are four state variables (denoted v_1, v_2, v_3, and v_4) associated with the gearbox model: the positions and velocities of the inputs and outputs to the gearbox; thus,

$$v_1 = \theta_m \tag{4a}$$

$$v_2 = \omega_m \tag{4b}$$

$$v_3 = \theta_o = \frac{\theta_g}{N_g} \tag{4c}$$

$$v_4 = \omega_o = \frac{\omega_g}{N_g} \tag{4d}$$

In the above equations, B_{in} represents the damping coefficient of the input shaft; B_g and k_g represent the damping and stiffness of the gearbox, respectively; B_1 represents the damping for the gearbox bearing; N_g represents the gear ratio of the gearbox; and J_m and J_g represent the moment of inertia of the input shaft and the composite moment of inertia of the gearbox, respectively.

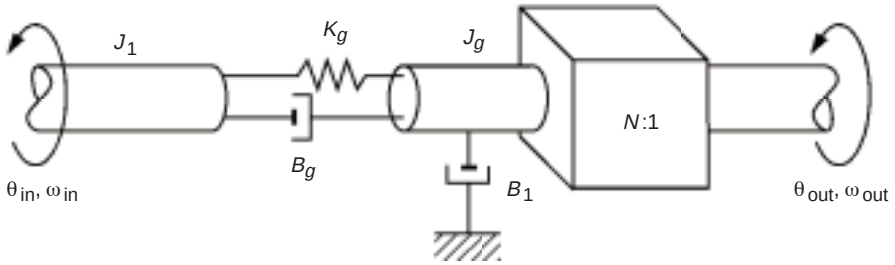

Fig. 7. Schematic model of the gear reducer using the input-stiffness model.

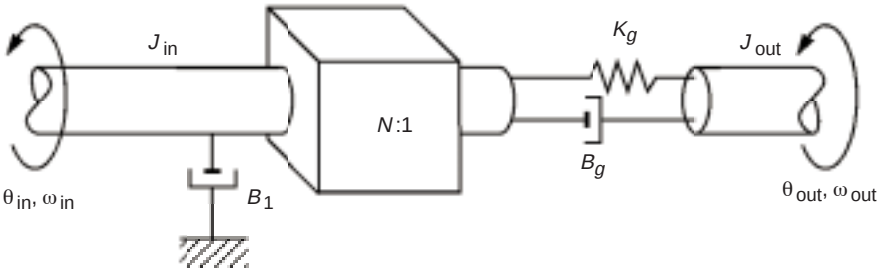

Fig. 8. Schematic model of the gear reducer using the output-stiffness model.

Each of the five independent drives in the subreflector drive assembly contains two gearbox models: one for the gear reducer and one for the ball screw. It is interesting to note that the gearbox and ball screw, though internally identical, have different inputs and outputs, namely,

(1) The gear reducer takes as its input the torque of the motor and the torque feedback from the ball screw; its outputs are the angle and velocity of the gear reducer output shaft.

(2) The ball screw, on the other hand, takes the acceleration of the reducer's shaft as input, along with the force required to move the subreflector at the given acceleration; its outputs are the subreflector position and velocity.

As a result, two unique state–space models are required to describe the two functionally similar devices. In addition to these differences, the ball screw's ratio, N_b, has units of radians per meter, rather than being a dimensionless relation between turns in and turns out of the gearbox.

The governing equations for the ball screw model are

$$J_b\dot{\omega}_b + B_2\omega_b = k_b(\theta_o - \theta_b) + B_b(\omega_o - \omega_b) + \frac{F_{\text{out}}}{N_b} \tag{5a}$$

$$F_{\text{out}} = -Ma \tag{5b}$$

where $a = \dot{\omega}_b/N_b$, and the state variables are as follows:

$$v_5 = x_{\text{out}} = \frac{\theta_b}{N_b} \tag{6a}$$

$$v_6 = v_{\text{out}} = \frac{\omega_b}{N_b} \tag{6b}$$

As in the gear reducer's case, the coefficients k_b and B_b represent the stiffness and damping factor, respectively, for the ball screw itself, while B_2 represents the damping in the ball screw's bearing. The J_b is the composite moment of inertia for the ball screw; N_b is the ball screw's ratio in radians per meter; and M is the total moving mass of the subreflector.

The concatenation of the two gearbox models is shown in Fig. 6. The subreflector, due to its small size, is assumed to be a rigid body. Because of the slight differences between the x-, y-, and z-axis mounts, the mass of each drive model is slightly different. The y-axis drive moves the center and bottom plates as well as the subreflector; the x-axis drive moves the bottom plate and the subreflector; and the z-axis drive moves the subreflector itself.

Combining the equations for the gearbox and the ball screw, one obtains the following state–space model for the complete drive dynamics:

$$\dot{x}_d = A_d x_d + B_d T_m \tag{7a}$$

$$y_d = C_d x_d \tag{7b}$$

The state x_d consists of six state variables,

$$x_d^T = [\, v_1 \quad v_2 \quad v_3 \quad v_4 \quad v_5 \quad v_6 \,] \tag{8}$$

They represent the equivalent states of the mechanical output of the gear reducer system and the mechanical input to the ball screw system. The input to the system is the torque from the motor, T_m; the outputs are the position and velocity of the subreflector in the given axis, $y_d = [x_{\text{out}} \quad v_{\text{out}}]^T$. The state matrices are as follows:

$$A_d = \begin{bmatrix} 0 & 1 & 0 & 0 & 0 & 0 \\ -\dfrac{k_g}{J_m} & -\dfrac{B_g + B_m}{J_m} & \dfrac{k_g N_g}{J_m} & \dfrac{B_g N_g}{J_m} & 0 & 0 \\ 0 & 0 & 0 & 1 & 0 & 0 \\ \dfrac{k_g}{J_g N_g} & \dfrac{B_g}{J_g N_g} & \dfrac{k_g N_g^2 - k_b}{J_g N_g^2} & \dfrac{(B_g - B_1) N_g^2 - B_b}{J_g N_g^2} & \dfrac{k_b N_b}{J_g N_g^2} & \dfrac{B_b N_b}{J_g N_g^2} \\ 0 & 0 & 0 & 0 & 0 & 1 \\ 0 & 0 & \dfrac{k_b}{N_b \mu} & \dfrac{B_b}{N_b \mu} & -\dfrac{k_b}{\mu} & -\dfrac{B_b + B_2}{\mu} \end{bmatrix} \tag{9a}$$

$$\left.\begin{aligned} B_d &= \begin{bmatrix} 0 \\ \dfrac{1}{J_m} \\ 0 \\ 0 \\ 0 \\ 0 \end{bmatrix} \\ C_d &= \begin{bmatrix} 0 & 0 & 0 & 0 & 1 & 0 \\ 0 & 0 & 0 & 0 & 0 & 1 \end{bmatrix} \end{aligned}\right\} \tag{9b}$$

where

$$\mu = J_b + \frac{M}{N_b^2} \tag{9c}$$

Finally, numerical constants were determined or approximated for the different components of the physical system and used as follows. The mass of the subreflector was 450 kg.

Physical data for the gearboxes and ball screw actuators were significantly harder to obtain than data for the motor and in many cases had to be approximated rather than obtained directly. The exact ratio of the gearbox was 6.196:1, according to documentation from the manufacturer. The inertia of the input shaft was 0.08 kgm^2. The approximate value of the shaft stiffness was obtained as an equivalent to the stiffness of a 0.5 m steel shaft of 1 cm radius. The actual shaft is much shorter and has a radius of 1.27 cm (or 1/2 in.) and so the actual shaft would be stiffer than this approximate value. No data were available for the damping ratios, and so they were approximated to be 1/10 of the motor shaft damping, or about 10^{-4} Nms/rad. It should be noted that despite the probable inaccuracy in these values, the mechanical modes of the gearbox linkage are at far higher frequencies than warrant concern in the design of the controller.

If the gearbox mechanical traits are of trivial significance to the drive system's behavior, the ball screw actuator is even more trivial, since its effects are tempered by the torque reduction of the gear reducer. This is fortunate, since data on the ball screws were less forthcoming than for the gear reducers. The only values known for certain were the input shaft inertia of 0.0022 kgm^2 and the gear ratios, which equate to 3779 input rotations per meter of movement (96 rotations per inch) for the x- and z-axis actuators and 2287 input rotations per meter (58.1 rotations per inch) for the y-axis actuator. The ball screws were assumed to be more rigid than the gear reducers, and so their stiffness was assigned the value of 10^4 Nm/rad, and the damping value of 10^{-4} Nms/rad was used again. Since the speed of the input shaft was negligible (only 58 rpm at a subreflector rate of 0.025 cm/s), damping was most likely insignificant.

The physical parameters for the gearbox and ball screw components are summarized in Table 3.

D. Combining the Amplifier, Motor, and Mechanical Subsystem Into the Rate Loop

The subreflector rate-loop model consists of the amplifier, motor, and mechanical subsystem. Its dynamics were simulated using the Simulink model, as shown in Fig. 2. The transfer function of the rate-loop model, from the rate command (m/s) to the transducer position (m) is shown in Fig. 9, and from the rate command to the tachometer (converted to an equivalent rate in m/s of the subreflector) is shown in Fig. 10. The figures show a bandwidth of 8 Hz and a resonance peak of 5 Hz.

Table 3. Gearbox and ball screw parameters.

Parameter	Gearbox	Ball screw
Ratio	$N_g = 6.196$	$N_b = 2287$ turns per m (y-axis) $N_b = 3779$ turns per m (x- and z-axes)
Input shaft inertia	$J_g = 0.08$ kgm^2	$J_b = 0.0022$ kgm^2
Input shaft stiffness	$k_g = 2500$ Nm/rad	$k_b = 10,000$ Nm/rad
Input shaft damping	$Bg = 0.0001$ Nms/rad	$B_b = 0.0001$ Nms/rad

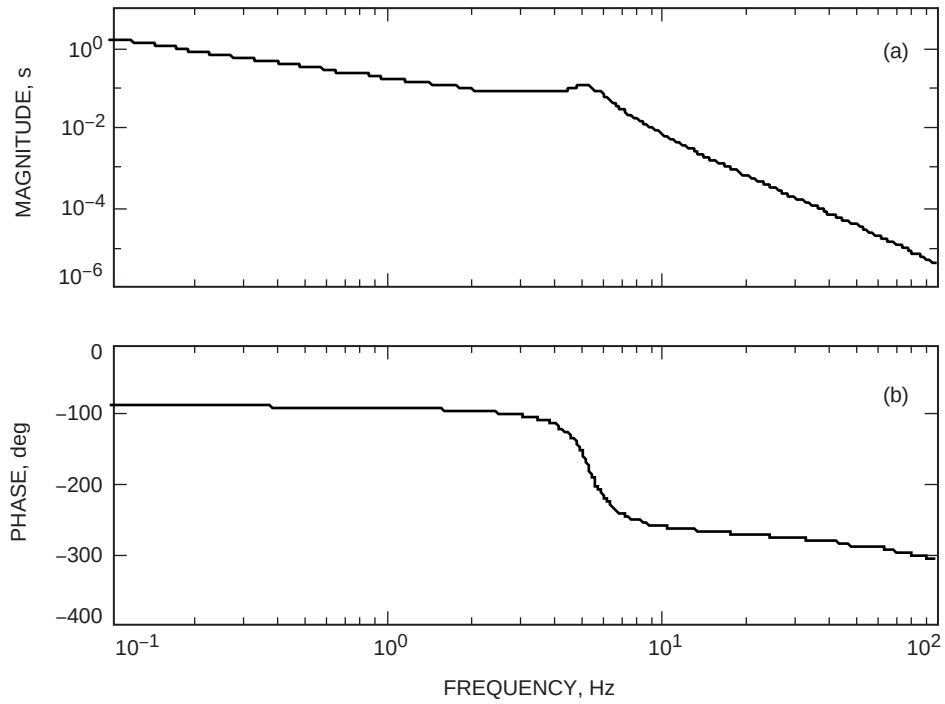

Fig. 9. Rate-loop transfer function from the rate command to the subreflector position: (a) magnitude and (b) phase.

The tachometer response to the step input is shown in Fig. 11. It shows 5 Hz oscillations and a 1 s settling time. The response of the transducer to a step input rate command is shown in Fig. 12. Again a slight resonance, tempered by the drive train, is visible at around 5 Hz, and again the subreflector's settling time is approximately 1 s.

IV. Closed-Loop Model and Performance

The controller used in this model has a simple proportional–integral (PI) architecture (shown in Fig. 13), followed by a scaling factor to convert from a position command (in inches) to volts of rate command to match voltage from the tachometer. Position command is in inches due to the antiquated nature of the equipment for which the controller was designed—both the computer command and the transducer feedback are scaled to inches—and to the familiarity of station personnel with the currently installed system of units.

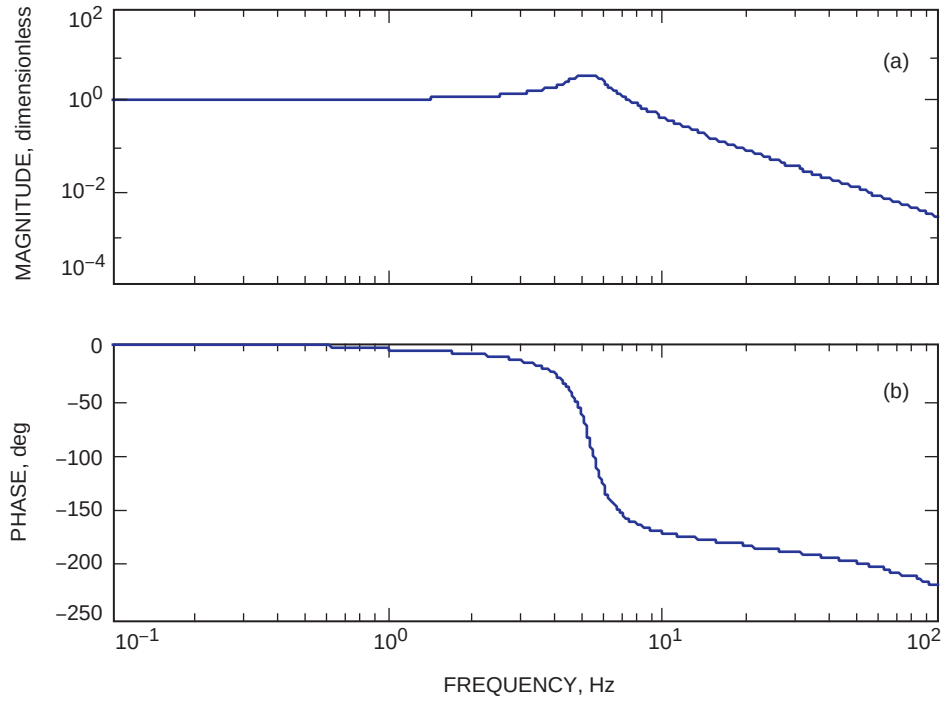

Fig. 10. Transfer function of the rate-loop model from the rate command to the tachometer: (a) magnitude and (b) phase.

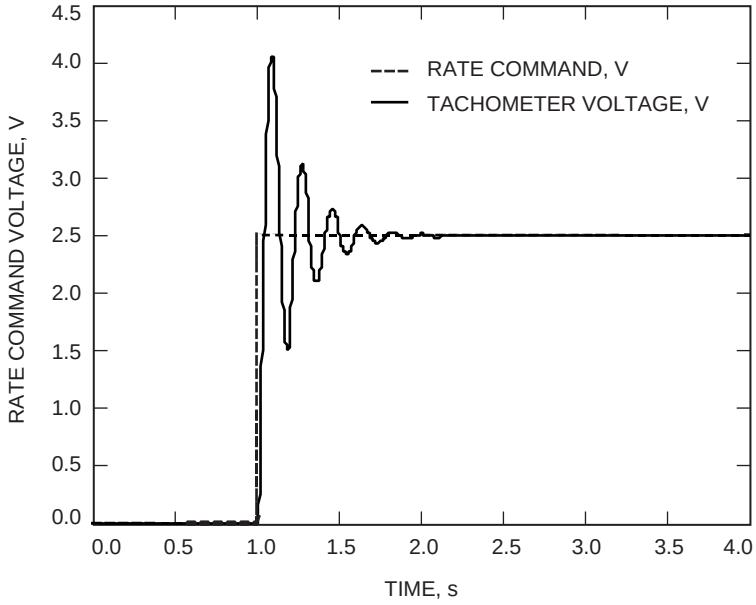

Fig. 11. Tachometer response of the rate-loop system to the step rate command.

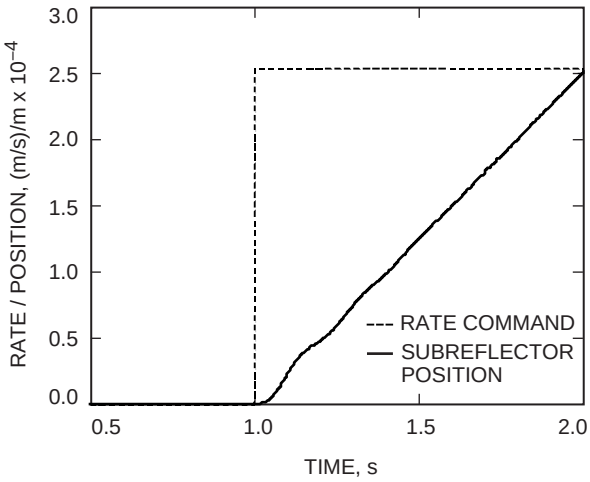

Fig. 12. Rate command and subreflector position response of the rate loop system.

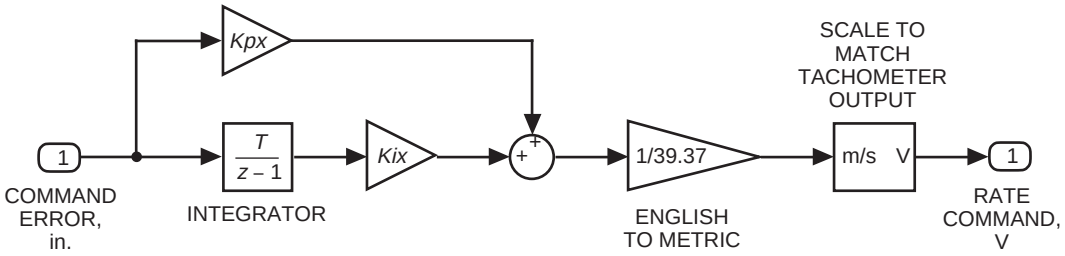

Fig. 13. Simulink model of the PI controller.

Designing a PI controller is equivalent to choosing the gains for the proportional and integral gains for the controller. The process utilized to accomplish this was an iterative one. We began with an integral gain of zero and experimented with different values of the proportional gain. A higher proportional gain will produce a more assertive response, but tends to cause the system to oscillate, and too high a proportional gain results in instability. On the other hand, too low a proportional gain leads to a sluggish reaction to commands. We found that the highest proportional gain that yielded a stable system was for $K_p = 10.0$. We then reduced the proportional gain from that point until the oscillations had minimized.

A proportional gain of 3.0 was chosen as a balance between response speed and oscillation. The proportional controller has a bandwidth of approximately 0.5 Hz and a settling time of 1.16 s (see Figs. 14 and 15). As expected, though the proportional-only controller responds acceptably to step commands, it results in steady-state errors when the command is a constant rate offset. To compensate for this problem, an integral term is added to the controller. Just as for the proportional gain, there are advantages and disadvantages to larger integral gains. A larger integral gain will increase the bandwidth; however, it also will cause the system to go into oscillations upon receiving a step command and will cause excessive overshoot.

In the case of integral gain, a balance was struck at $K_i = 3.3$, while maintaining K_p at 3.0. For this value, the bandwidth of the system was 0.7 Hz, the settling time was 2.60 s, and the overshoot was 17.7 percent (see Figs. 16 and 17).

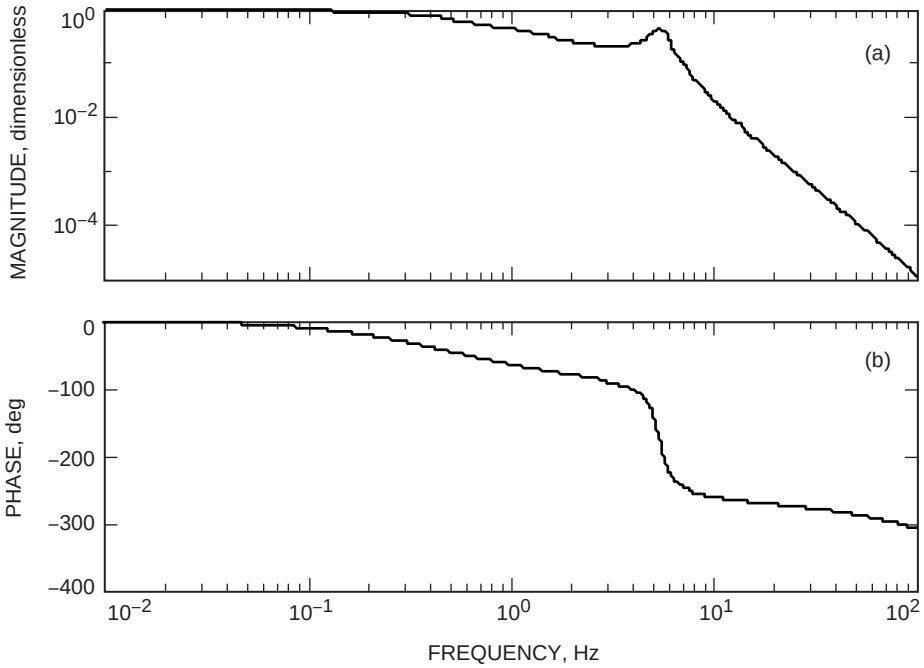

Fig. 14. Transfer function of the closed-loop system with proportional controller: (a) magnitude and (b) phase.

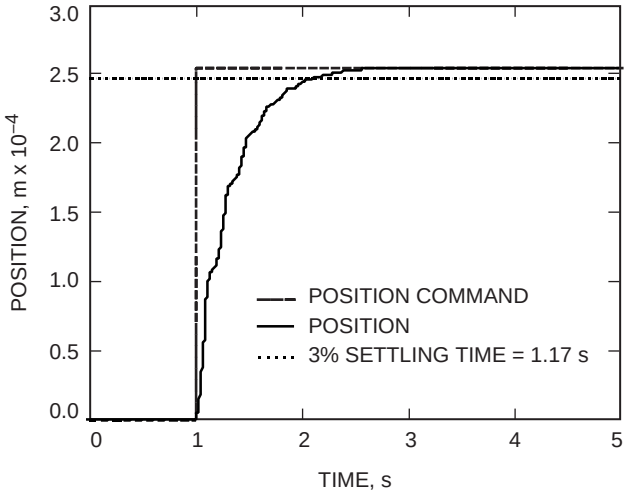

Fig. 15. Step response of the closed-loop system with proportional controller.

V. Conclusions

This article presented the procedure for analysis of the open- and closed-loop dynamics of the HEF subreflector. It is a tool for evaluation of the subreflector performance, correction of its hardware to meet the required performance, and selection of the controller gains. It also analyzed in detail the open- and closed-loop dynamics of the subreflector. The simulation results show that the open-loop dynamics are acceptable and that closed-loop dynamics settling time is 2.60 s, overshoot is 17.7 percent, and bandwidth is 0.7 Hz. The antenna servo in azimuth and elevation has similar parameters in terms of settling time, overshoot, and bandwidth; thus, we conclude that the closed-loop dynamics of the subreflector are satisfactory.

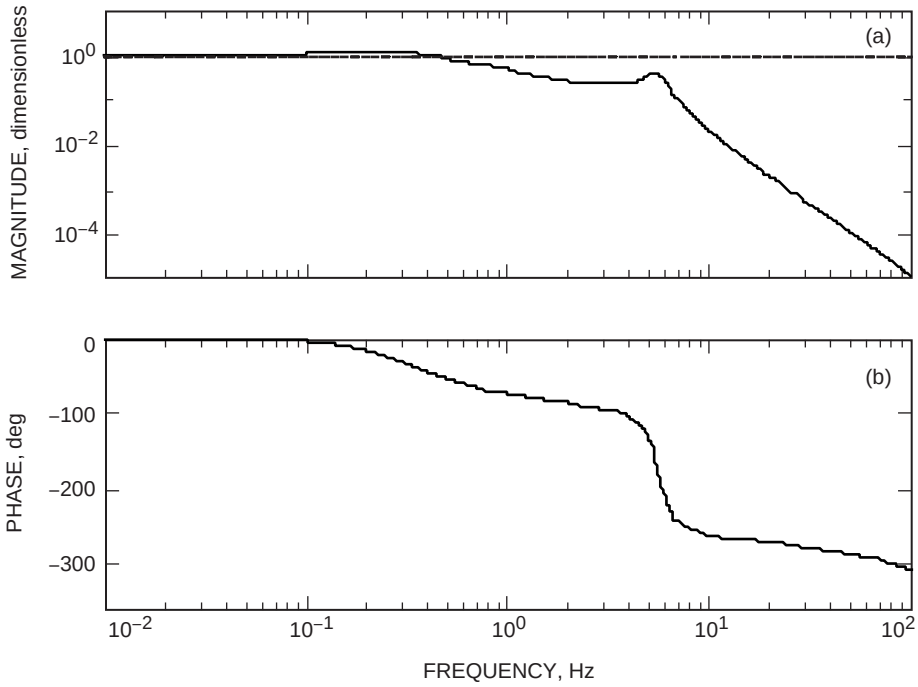

Fig. 16. Transfer function of the closed-loop system with PI controller: (a) magnitude and (b) phase.

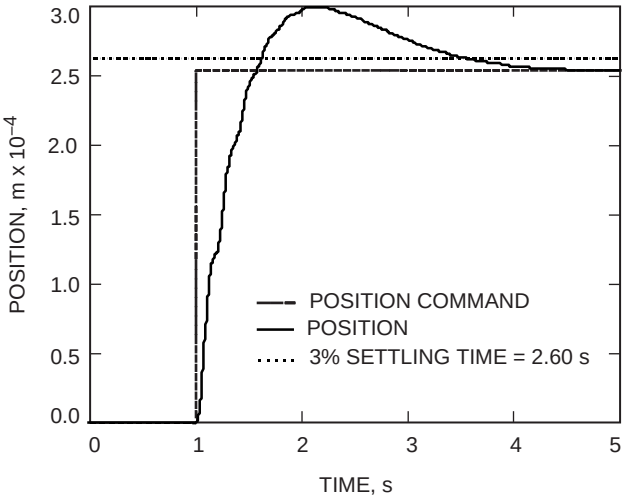

Fig. 17. Step response of the closed-loop system with PI controller.